Wireless Power Transfer Closed-Loop Control for Low-Power Active Implantable Medical Devices

Wireless Power Transfer Closed-Loop Control for Low-Power Active Implantable Medical Devices

Fabiana Del Bono*, Andrea Bontempi*, Nicola Di Trani†, Danilo Demarchi*,
Alessandro Grattoni† and Paolo Motto Ros*
*Dept. of Electronics and Telecommunications, Politecnico di Torino, Turin, Italy
†Dept. of Nanomedicine, Houston Methodist, Houston, Texas
fabiana.delbono@polito.it

***Abstract*—Near-field resonant inductive coupling is the most mature wireless power transfer (WPT) method for implantable medical devices. Common commercial WPT components are not optimized neither to deliver small amounts of power nor to work with other than small air gaps. In this paper, a closed-loop control is integrated with commercial off-the-shelf WPT components to efficiently recharge and power an implantable device for controlled active drug delivery. The system keeps the transmitted power stable and reliable, achieving a 26 % transfer efficiency with delivered power of tens of milliwatts, guaranteeing an autonomy of 5 days with a 4-hour recharge. Overheating is kept around the 2 °C safety limit.**

***Index Terms*—Active implantable medical devices (AIMDs), wireless power transfer (WPT), near-resonant inductive coupling (NRIC), nanochannel Delivery System (nDS)**

I. Introduction

The operation of active implantable medical devices (AIMDs) is generally guaranteed by batteries, which occupy most of the device's space [1], [2]. In the majority of implantable systems, volume constraints are of utmost importance in regard to device discreetness and patient acceptability [3], [4], much more than for wearable IoT devices. Next-generation AIMDs aim to minimize the overall size and power consumption and improve efficacy and safety [5], eventually including connectivity to allow the exchange of information and personalize therapy [6], [7]. The need for miniaturization and the increased power demand required by communication limit the use of primary batteries. Secondary batteries can minimize the overall size with the advantage that they can be recharged periodically. For this purpose, AIMDs must be equipped with a wireless power transfer (WPT) system [8]. Among WPT methods [1], [9]–[11], near-resonant inductive coupling (NRIC) systems allow transmitting power from tens to hundreds of milliwatts, with an operating range of the order of the skin's thickness. This technology is mature and is already used in powering some categories of commercial AIMDs [12]. This makes it suitable to be integrated into experimental subcutaneous implants to recharge secondary batteries, using receiving coils with diameter lower than 2 cm. The main problem of the NRIC system is overheating the coils and integrated circuits (ICs), especially in the case of commercial components [13]. European Standard EN45502-1 [14] requires that the temperature of an implanted device does not exceed the limit of 2 °C above body temperature. Overheating is due to poor power transfer efficiency (PTE) of the NRIC system and the low quality factor of coils. The PTE is affected by load variation, misalignment and detuning of the coils [11], [15], and is significantly reduced when the transmitted power decreases [16]. This paper presents a NRIC system for power transfer management in subcutaneous biomedical implants (Fig. 1). The system is employed to recharge a secondary battery and power supply the nanochannel Delivery System (nDS), a remotely controlled nanofluidic implantable platform for tunable drug delivery featuring Bluetooth Low Energy (BLE) connectivity [7], [17]. The NRIC system is made of commercial off-the-shelf (COTS) WPT components, used beyond datasheet recommendations. The aim is to overcome their limited reliability and efficiency [18] when delivering power to the load in the order of tens of milliwatts at subcutaneous tissue distances. A closed-loop is introduced to maximise efficiency and guarantee continuity of power transfer, limiting power dissipation and avoiding overheating.

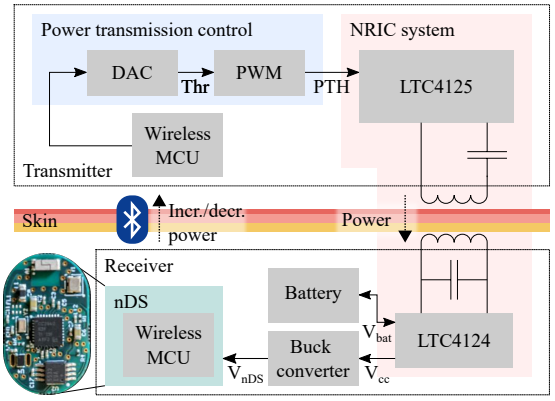

Fig. 1. Overview of the system. An external power transmitter delivers power to the subcutaneous implant via a NRIC link. The implanted battery is recharged while continuously powering the nDS device. The nDS MCU measures the received power levels and provides feedback to the transmitter MCU via BLE. A control circuit is used to regulate the transmitted power accordingly.

II. Materials and Methods

The WPT NRIC system is based on two ICs, an AD LTC4125 for the transmitter (TX) and an AD LTC4124 for the receiver (RX). The LTC4124 occupies a minimum area of

4 mm^2 and requires only two external passive components with respect to similar solutions. The LC tank of the TX consists of the coil and two parallel capacitors in series with it. The coil (Wurth Electronic, 760308101104) has an inductance of 6.8 µH, and a diameter of 20.8 mm. The LC tank of the RX is composed of a coil and capacitor in parallel. The coil (Wurth Electronic, 760308101220) has an inductance of 12.6 µH, a diameter of 17 mm. The resonance frequency of the NRIC system is tuned at 200 kHz, with the quality factor of TX and RX coils 60.9 and 25, respectively. All the nominal values reported are from datasheets. The DC2770A-B evaluation kit has been used to test the NRIC system.

The TX IC has its control system but does not directly involve the specific RX. In fact, the LTC4125 works by periodically performing a stepwise linear ramp of transmitted power to detect the presence or absence of a valid receiver. The IC monitors whether there is a voltage increase on the LC tank above a hardware-set threshold. If not, power transmission is interrupted. Closed-loop control, split between TX and RX (each with an MCU connected via BLE, see Fig. 1), is therefore needed to avoid this problem in critical operating conditions and better manage power delivery [19]. The MCU of the nDS (RX) monitors two conditions (1) and (2).

$$V_{CC} > 3.6\,\mathrm{V} \tag{1}$$

$$V_{BAT} + 300\,\mathrm{mV} < V_{CC} < V_{BAT} + 700\,\mathrm{mV} \tag{2}$$

V_{BAT} is the battery voltage, and V_{CC} is the rectified output voltage (not regulated) of the LTC4124. To ensure that a proper amount of power is delivered during recharge, V_{CC} should fall in a specific range above V_{BAT}. The RX sends a periodic Bluetooth notification advising whether to increase or decrease the transmitted power if conditions are not met, so to keep V_{CC} stable as much as possible, with the ultimate goal of avoiding excessive or insufficient power delivery. Fig. 2 shows the operation of the power transmission control on the TX. The voltage on PTH controls the power transmitted by the LTC4125. The voltage is regulated by discharging or charging the capacitor via the external pull-down resistor or integrated pull-up resistor, respectively. The voltage on the capacitor is kept stable around the threshold value set by the DAC. The threshold is modified by the DAC with steps of 2.5 mV.

First, the system was characterized, tracing transmission efficiency with varying coil distances and battery voltages, and compared with the corresponding open-loop system. The battery under recharge was simulated by connecting a DC power supply to a R_{BAT} 20 Ω resistor at the battery pin of the power RX, with voltage swept from 2.8 V to 4.1 V with a step size of 100 mV.

Battery charging was then set up in two cases, with and without connection with the nDS. Coin batteries with different capacity (16 mAh to 40 mAh) and recharge current (10 mA to 25 mA), similar size, were used for the tests. The test bench included the system as shown in Fig. 1, a DC Power supply to power the TX, and an external MCU connected to RX and TX modules for real-time data collection. V_{THR} and NTC

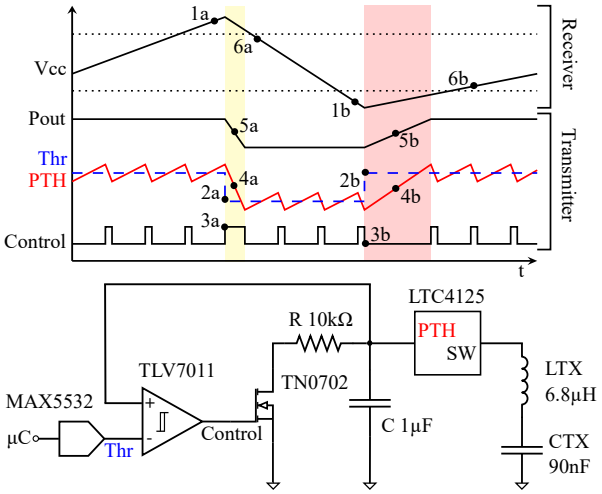

Fig. 2. (top) Representation of the control system's operation when the V_{CC} RX voltage increases/decreases (a/b): 1a/b) measurement of V_{CC} RX voltage and BLE notification; 2a/b) change of threshold Thr value; 3a/b) control activation; 4a/b) PTH voltage variation; 5a/b) power transmission variation. 6a/b) V_{CC} voltage returns within the range. (bottom) The simplified electrical circuit schematic of the TX control system.

voltage for coil temperature were continuously measured on TX, V_{CC}, V_{BAT}, I_{BAT}, and V_{nDS} (in the second case) on the RX. Additionally, periodic RX circuit thermal imaging and readings of the total power supplied to the transmitter P_{TX} were performed. Overall efficiency is calculated as

$$\eta = \eta_{TX} \cdot \eta_{link} \cdot \eta_{RX} = (P_{BAT} + P_{nDS})/P_{TX} \tag{3}$$

with $P_{BAT} = V_{BAT} \times I_{BAT}$ the power used to recharge the battery and $P_{nDS} = V_{nDS} \times I_{nDS}$ the regulated power (through a Buck converter) provided to the nDS (average I_{nDS} is 5 mA with the BLE connection active).

III. Experimental Results and Discussion

Results on transmission efficiency are reported in Fig. 3, comparing open and closed-loop. In Fig. 3a, the open loop control shows discontinuous operation; the efficiency is 0 % for those distances where the TX cannot correctly detect the receiver and, therefore, no power is transmitted. In closed-loop (Fig. 3b), power transfer is always successfully performed, and no fault conditions occur on the TX side. Efficiency values result to be higher when higher battery voltage is reached, and show a peak for distances compatible with skin thickness. Despite a higher coupling coefficient at shorter distances, η_{TX} and η_{RX} in eq. 3 may indeed maximise the overall η at a higher P_{TX}, increasing with distance [20]. Inductive coupling is mildly robust, maintaining efficiencies higher than 15 % within 2 mm of lateral misalignment, corresponding to 20 % of the TX coil radius, and higher than 10 % in the case of 3.5° angular misalignment, both in the case of coil distance fixed to 6.5 mm (Fig. 4). A slight but not meaningful decrease in efficiency is shown with biological tissue (chicken breast) interposed between the coils. The tissue also reduces overheating in correspondence of both the coils and the receiver IC.

TABLE I
CLOSED LOOP SYSTEM PERFORMANCE DURING LIR2025 CHARGING TESTS AT 10 mA, MEASURED AT DIFFERENT DISTANCES d BETWEEN THE TX AND THE RX, WITH AND WITHOUT THE DRUG DELIVERY SYSTEM *nDS*.

***d* (mm)**	***nDS***	P_{TX} ***max.* (mW)**	P_{RX} ***max.* (mW)**	η_{AVG} **(%)**	V_{THR} ***max.* (mV)**	ΔT_{TX} ***max.*(°C)**	ΔT_{RX} ***max.*(°C)**
2.5	Yes	250	64.9	23.9	279.0	2.5	2.1
6.5	No	160	40.0	21.3	221.0	1.3	2.0
6.5	Yes	210	65.4	26.0	270.7	2.1	1.4

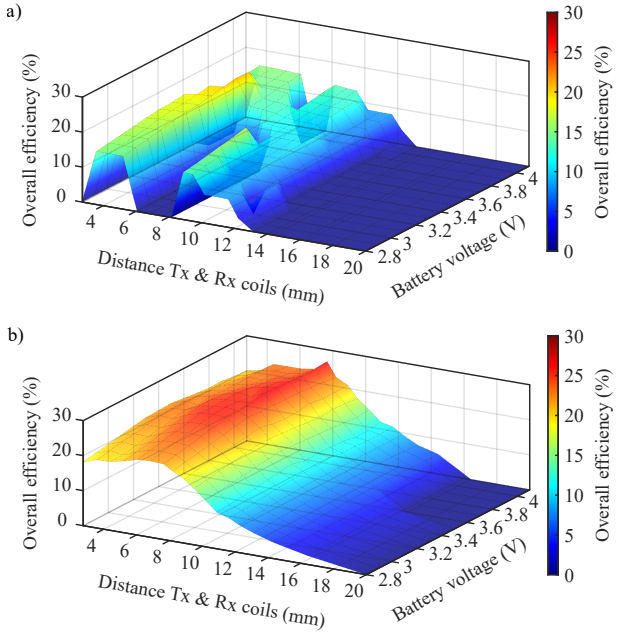

Fig. 3. Comparison of power transfer efficiency of the NRIC WPT system without (a) and with (b) the closed-loop. In (a), 0 % efficiency means that the TX can not find the RX and therefore does not deliver power. Test conducted in air, charging current 10 mA, coil distance 2.5–20 mm, simulated battery.

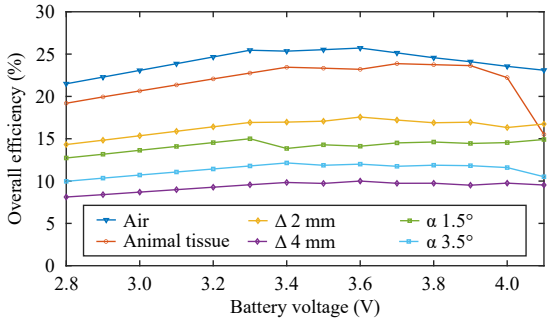

Fig. 4. Efficiency in case of lateral and angular misalignment and interposed animal tissue. Charging current 10 mA, distance 6.5 mm, simulated battery. Misalignment tests are performed in air to achieve greater accuracy regard the experimental set-up.

While this behaviour needs to be further investigated, it may be explained by the thermal capacitance of the water content in the tissue, and is expected to be further enhanced in presence of the blood circulation of an an in-vivo environment. Tests on battery charging evidence a smooth charging process, again with no occurrence of fault conditions and interruptions, in line with the theoretical CC-CV charging profile [21]. Data obtained in these tests led to selecting a 25 mAh battery (LIR2025) with a charging current of 10 mA as the best compromise between TX power, overheating, battery size, charging current, and interval between recharges. Complete battery charging is achieved within 250 min; results of the continuous monitoring are summarized in Table I. Tests with nDS show complete functionality of the drug delivery system during the whole recharge process. In this case, supplied power increases according to the power demand of the device; however, the maximum overheating remains around the safety limits for an in-vivo application, even not considering the stabilising effect of the biologic environment on the temperature.

TABLE II
COMPARISON WITH SIMILAR NRIC SOLUTIONS, $P_{TX} < 1$ W AND 30 kHz TO 300 kHz (LF BAND) OPERATING FREQUENCY

Reference	P_{TX} ***(mW)***	***freq. (kHz)***	η **(%)**	***Application***
[26]	1000	206	12.5	General
[27]	810	125	29.9	Neural
This work	210	200	26.0	Drug delivery

Performance comparison with other low-power WPT systems operating in the same frequency range is reported in Table II. Overall efficiency is between 25 % and 30 %, a good result considering that similar low-power WPT systems (Table II) exhibit reduced efficiency as well (smaller than the efficiency reported for higher power related WPT systems, e.g., [22], [23]). More importantly, measured performance is consistent across all the recharge process (Fig. 3b) and with respect to lateral and angular misalignment and the interposed animal tissue (Fig. 4). Finally, thermal verification of the WPT system is a critical requirement in biomedical applications, rarely reported and difficult to meet [18]: in this regard, the proposed system shows very promising results (Table I).

IV. CONCLUSIONS

A closed-loop wireless power transfer system made of commercial off-the-shelf components was developed and tested with an experimental AIMD for in-vivo applications. Experimental results show the stability of power transfer, with limited overheating and suitable efficiency. The recharge of a 25 mAh battery allows the activity of the drug delivery system for at least 5 days, based on the previous estimate on the device presented in [7], that relies on a 90 mAh primary cell (CR2016). Results are promising in the perspective of a long-term implant for chronic animal studies [24], [25]. The chosen battery allows for up to 500 recharge cycles for a total projected chronic duration of more than 6 years.

REFERENCES

[1] K. Agarwal, R. Jegadeesan, Y.-X. Guo, and N. V. Thakor, "Wireless power transfer strategies for implantable bioelectronics," *IEEE Reviews in Biomedical Engineering*, vol. 10, pp. 136–161, 2017.

[2] J. S. Ho, S. Kim, and A. S. Y. Poon, "Midfield wireless powering for implantable systems," *Proceedings of the IEEE*, vol. 101, no. 6, pp. 1369–1378, 2013.

[3] F. P. Pons-Faudoa, A. Sizovs, K. A. Shelton, Z. Momin, J. A. Niles, L. R. Bushman, J. Xu, C. Y. X. Chua, J. E. Nichols, S. Demaria, M. M. Ittmann, T. Hawkins, J. F. Rooney, M. A. Marzinke, J. T. Kimata, P. L. Anderson, P. N. Nehete, R. C. Arduino, M. Ferrari, K. J. Sastry, and A. Grattoni, "Preventive efficacy of a tenofovir alafenamide fumarate nanofluidic implant in shiv-challenged nonhuman primates," *Advanced Therapeutics*, vol. 4, no. 3, p. 2000163, 2021.

[4] F. P. Pons-Faudoa, A. Ballerini, J. Sakamoto, and A. Grattoni, "Advanced implantable drug delivery technologies: transforming the clinical landscape of therapeutics for chronic diseases," *Biomedical Microdevices*, vol. 21, no. 2, p. 47, May 2019.

[5] J. S. Ho, A. J. Yeh, E. Neofytou, S. Kim, Y. Tanabe, B. Patlolla, R. E. Beygui, and A. S. Y. Poon, "Wireless power transfer to deep-tissue microimplants," *Proceedings of the National Academy of Sciences*, vol. 111, no. 22, pp. 7974–7979, 2014.

[6] G. Bruno, G. Canavese, X. Liu, C. S. Filgueira, A. Sacco, D. Demarchi, M. Ferrari, and A. Grattoni, "The active modulation of drug release by an ionic field effect transistor for an ultra-low power implantable nanofluidic system," *Nanoscale*, vol. 8, pp. 18 718–18 725, 2016.

[7] N. Di Trani, A. Silvestri, G. Bruno, T. Geninatti, C. Y. X. Chua, A. Gilbert, G. Rizzo, C. S. Filgueira, D. Demarchi, and A. Grattoni, "Remotely controlled nanofluidic implantable platform for tunable drug delivery," *Lab Chip*, vol. 19, pp. 2192–2204, 2019.

[8] Y. Zhou, C. Liu, and Y. Huang, "Wireless power transfer for implanted medical application: A review," *Energies*, vol. 13, 6 2020.

[9] G. L. Barbruni, P. M. Ros, D. Demarchi, S. Carrara, and D. Ghezzi, "Miniaturised wireless power transfer systems for neurostimulation: A review," *IEEE Transactions on Biomedical Circuits and Systems*, vol. 14, no. 6, pp. 1160–1178, 2020.

[10] A. N. Khan, Y.-O. Cha, H. Giddens, and Y. Hao, "Recent advances in organ specific wireless bioelectronic devices: Perspective on biotelemetry and power transfer using antenna systems," *Engineering*, vol. 11, pp. 27–41, 2022.

[11] S. R. Khan, S. K. Pavuluri, G. Cummins, and M. P. Desmulliez, "Wireless power transfer techniques for implantable medical devices: A review," *Sensors (Switzerland)*, vol. 20, pp. 1–58, 6 2020.

[12] M. Haerinia and R. Shadid, "Wireless power transfer approaches for medical implants: A review," *Signals*, vol. 1, pp. 209–229, 12 2020.

[13] I. Williams, A. Rapeaux, J. Pearson, K. Nazarpour, E. Brunton, S. Luan, Y. Liu, and T. G. Constandinou, "Senseback – implant considerations for an implantable neural stimulation and recording device," in *2019 IEEE Biomedical Circuits and Systems Conference (BioCAS)*, 2019, pp. 1–4.

[14] "En 45502-1 active implantable medical devices – part 1: General requirements for safety, marking and information to be provided by the manufacturer." 1997.

[15] H. J. Kim, H. Hirayama, S. Kim, K. J. Han, R. Zhang, and J. W. Choi, "Review of near-field wireless power and communication for biomedical applications," *IEEE Access*, vol. 5, pp. 21 264–21 285, 9 2017.

[16] R. Shadid and S. Noghanian, "A literature survey on wireless power transfer for biomedical devices," *International Journal of Antennas and Propagation*, vol. 2018, 2018.

[17] A. Silvestri, N. Di Trani, G. Canavese, P. Motto Ros, L. Iannucci, S. Grassini, Y. Wang, X. Liu, D. Demarchi, and A. Grattoni, "Silicon carbide-gated nanofluidic membrane for active control of electrokinetic ionic transport," *Membranes*, vol. 11, no. 7, 2021.

[18] I. Williams, E. Brunton, A. Rapeaux, Y. Liu, S. Luan, K. Nazarpour, and T. G. Constandinou, "Senseback - an implantable system for bidirectional neural interfacing," *IEEE Transactions on Biomedical Circuits and Systems*, vol. 14, no. 5, pp. 1079–1087, 2020.

[19] W. Li, "Close the loop between wireless charger receiver and transmitter without digital controllers," Analog Devices, Tech. Rep., 2022.

[20] P. Pérez-Nicoli, F. Silveira, and M. Ghovanloo, *Inductive Links for Wireless Power Transfer*. Springer International Publishing, 2021.

[21] E. Ayoub and N. Karami, "Review on the charging techniques of a li-ion battery," in *2015 Third International Conference on Technological Advances in Electrical, Electronics and Computer Engineering (TAEECE)*, 2015, pp. 50–55.

[22] A. Ghahary and B. Cho, "Design of transcutaneous energy transmission system using a series resonant converter," *IEEE Transactions on Power Electronics*, vol. 7, no. 2, pp. 261–269, 1992.

[23] G. B. Joun and B. Cho, "An energy transmission system for an artificial heart using leakage inductance compensation of transcutaneous transformer," *IEEE Transactions on Power Electronics*, vol. 13, no. 6, pp. 1013–1022, 1998.

[24] A. Grattoni, D. Fine, A. Ziemys, J. Gill, E. Zabre, R. Goodall, and M. Ferrari, "Nanochannel systems for personalized therapy and laboratory diagnostics," *Current Pharmaceutical Biotechnology*, vol. 11, no. 4, pp. 343–365, 2010.

[25] N. Di Trani, A. Silvestri, A. Sizovs, Y. Wang, D. R. Erm, D. Demarchi, X. Liu, and A. Grattoni, "Electrostatically gated nanofluidic membrane for ultra-low power controlled drug delivery," *Lab Chip*, vol. 20, pp. 1562–1576, 2020.

[26] M. A. Adeeb, A. B. Islam, M. R. Haider, F. S. Tulip, M. N. Ericson, and S. K. Islam, "An inductive link-based wireless power transfer system for biomedical applications," *Active and Passive Electronic Components*, vol. 2012, 2012.

[27] M. Ghovanloo and S. Atluri, "A wide-band power-efficient inductive wireless link for implantable microelectronic devices using multiple carriers," *IEEE Transactions on Circuits and Systems I: Regular Papers*, vol. 54, no. 10, pp. 2211–2221, 2007.